Inorg. Chem. **2007**, *46*, 5596–5607

Identification of the Radical Anions of $C_2N_4S_2$ and $P_2N_4S_2$ Rings by In Situ EPR Spectroelectrochemistry and DFT Calculations

René T. Boeré,*,† Alan M. Bond,‡ Tristram Chivers,*,§ Stephen W. Feldberg,|| and Tracey L. Roemmele†,§

Department of Chemistry and Biochemistry, University of Lethbridge, Lethbridge, Alberta T1K 3M4, Canada, School of Chemistry, Monash University, Clayton 3800, Victoria, Australia, Department of Chemistry, University of Calgary, Calgary, Alberta T2N 1N4, Canada, and Chemistry Department, Brookhaven National Laboratory, Upton, New York 11973

Received February 7, 2007

The previously unknown radical anions of unsaturated $E_2N_4S_2$ ring systems (E = RC, R_2NC, R_2P) can be generated voltammetrically by the one-electron reduction of the neutral species and, despite half-lives on the order of a few seconds, have been unambiguously characterized by electron paramagnetic resonance (EPR) spectroelectrochemistry using a highly sensitive in situ electrolysis cell. Cyclic voltammetric studies using a glassy-carbon working electrode in CH_3CN and CH_2Cl_2 with $[^nBu_4N][PF_6]$ as the supporting electrolyte gave reversible formal potentials for the $[E_2N_4S_2]^{0/-}$ process in the range of –1.25 to –1.77 V and irreversible peak potentials for oxidation in the range of 0.66 to 1.60 V (vs the $Fc^{+/0}$ couple; Fc = ferrocene). Reduction of the neutral compound undergoes an electrochemically reversible one-electron transfer, followed by the decay of the anion to an unknown species via a first-order (chemical) reaction pathway. The values of the first-order rate constant, k_f, for the decay of all the radical anions in CH_2Cl_2 have been estimated from the decay of the EPR signals for $(X–C_6H_4CN_2S)_2^{\bullet-}$, where X = 4-$OCH_3$ ($k_f = 0.04\ s^{-1}$), 4-CH_3 ($k_f = 0.02\ s^{-1}$), 4-H ($k_f = 0.08\ s^{-1}$), 4-Cl ($k_f = 0.05\ s^{-1}$), 4-CF_3 ($k_f = 0.05\ s^{-1}$), or 3-CF_3 ($k_f = 0.07\ s^{-1}$), and for $[(CH_3)_3CCN_2S]_2^{\bullet-}$ ($k_f = 0.02\ s^{-1}$), $[(CH_3)_2NCN_2S]_2^{\bullet-}$ ($k_f = 0.05\ s^{-1}$), and $[(C_6H_5)_2PN_2S]_2^{\bullet-}$ ($k_f = 0.7\ s^{-1}$). Values of k_f for X = 4-H and for $[(CH_3)_2NCN_2S]_2^{\bullet-}$ were also determined from the cyclic voltammetric responses (in CH_2Cl_2) and were both found to be $0.05\ s^{-1}$. Possible pathways for the first-order anion decomposition that are consistent with the experimental observations are discussed. Density functional theory calculations at the UB3LYP/6-31G(d) level of theory predict the structures of the radical anions as either planar (D_{2h}) or folded (C_{2v}) species; the calculated hyperfine coupling constants are in excellent agreement with experimental results. Linear correlations were observed between the voltammetrically determined potentials and both the orbital energies and Hammett coefficients for the neutral aryl-substituted rings.

Introduction

Many unsaturated compounds containing sulfur−nitrogen bonds are redox active.[1] Despite the fact that such rings and cages are typically quite electron rich, the formation of anions is usually facile, a phenomenon attributed to the high electronegativity of both nitrogen and sulfur.[2] We have published a comprehensive and critical review of the electrochemical data for compounds in this class.[3] Many of the most stable redox processes involve odd-electron intermediates that are neutral. However, diamagnetic species can also often be oxidized and/or reduced to cationic or anionic radicals.[4] One such ring system is 1,5,2,4,6,8-dithiatetrazocine, which has been characterized by crystallography in the planar forms **1** and **2** or in the folded form **3**, depending on the 3,7 substituents (Chart 1).[5] The closely related diphosphadithi-

* To whom correspondence should be addressed. E-mail: boere@uleth.ca (R.T.B.), chivers@ucalgary.ca (T.C.). Tel.: (403) 329-2045 (R.T.B.), (403) 220-5741 (T.C.). Fax: (403) 329-2057 (R.T.B.), (403) 289-9488 (T.C.).
† University of Lethbridge.
‡ Monash University.
§ University of Calgary.
|| Brookhaven National Laboratory.

(1) Chivers, T. *A Guide to Chalcogen-Nitrogen Chemistry*; World Scientific Publishing Co.: Singapore, 2005.

(2) Oakley, R. T. *Prog. Inorg. Chem.* **1988**, *36*, 299.

(3) Boeré, R. T.; Roemmele, T. L. *Coord. Chem. Rev.* **2000**, *210*, 369.

10.1021/ic070243t CCC: $37.00
Published on Web 06/07/2007

Chart 1. Chemical Structures for Compounds **1a**−**f**, **2**, **3**, and **4**

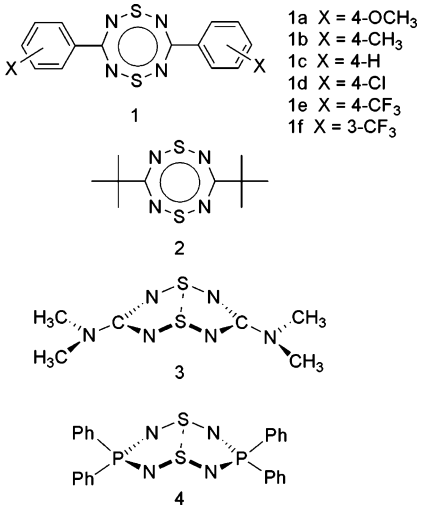

Scheme 1

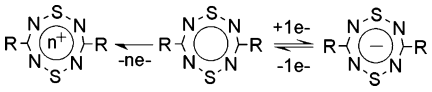

atetrazocine **4** and other analogues have only been characterized in the folded form.[6] There is an important analogy between the folded molecules **3** and **4** and the well-known cage molecule S_4N_4 in that they share similar transannular S···S contacts from the cross-ring in-phase overlap of high-lying N═S═N π^* orbitals. Thus both **3**[7] and **4**[8] have been extensively studied as model systems to investigate the complex chemical behavior of S_4N_4.

In a previous voltammetric investigation, reversible reduction and irreversible oxidation processes (Scheme 1) were detected for both folded and planar dithiatetrazocines **1**−**3**.[5b] The small variation in the reversible redox potentials for the reduction processes observed with various 3,7 substituents was attributed to the nature of the lowest-unoccupied molecular orbital (LUMO) of the neutral molecule, which is nodal at carbon and only transmits weak inductive influences from the substituents (Figure 1b). By contrast, the highest-occupied molecular orbital (HOMO) has a large ring carbon coefficient, which was used to explain the strong substituent dependence of the oxidation peak potentials (Figure 1a).[5b]

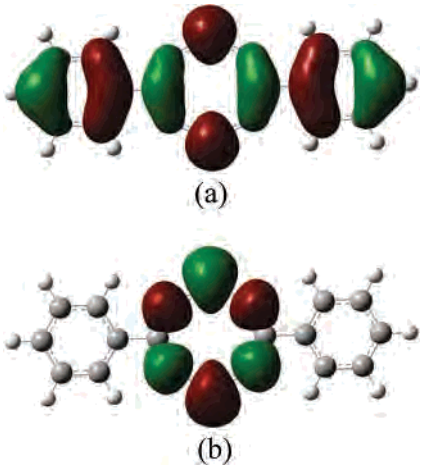

Figure 1. Kohn−Sham orbital isosurfaces of the redox π orbitals for (a) oxidation (HOMO) and (b) reduction (LUMO) of **1c**.

The number of electrons transferred in these processes has not been independently verified, and repeated efforts in our laboratory have failed to isolate the putative radical anions from chemical reductions of **1**−**3**, despite the apparent voltammetric reversibility of these processes. An earlier, cursory, electrochemical study of **4** by cyclic voltammetry in CH_3CN reported only that the radical anion is "short-lived ($t_{1/2} = 2-3$ s)".[9a] On the other hand, an extensive chemistry

(4) (a) Strom, E. T.; Russell, G. A. *J. Am. Chem. Soc.* **1965**, *87*, 3326. (b) Kwan, C. L.; Carmack, M.: Kochi, J. K. *J. Phys. Chem.* **1976**, *80*, 1786. (c) Atherton, J. N. M.; Ockwell, J. N.; Dietz, R. *J. Chem. Soc. A* **1967**, 771. (d) Wolmershäuser, G.; Schnauber, M.; Wilhelm, T. *Synth. Met.* **1986**, *14*, 239. (e) Cameron, T. S.; Haddon, R. C.; Mattar, S. M.; Parsons, S.; Passmore, J.; Ramirez, A. P. *Inorg. Chem.* **1992**, *31*, 2274. (f) Barclay, T. M.; Cordes, A. W.; Goddard, J. D.; Mawhinney, R. C.; Oakley, R. T.; Preuss, K. E.; Reed, R. W. *J. Am. Chem. Soc.* **1997**, *119*, 12136. (g) Boyle, P. D.; Parsons, S.; Passmore, J.; Wood, D. J. *J. Chem. Soc., Chem. Comm.* **1993**, 199. (h) Hunter, J. A.; King, B.; Lindsell, W. E.; Neish, M. A. *J. Chem. Soc., Dalton Trans.* **1980**, 880. (i) Barclay, T. M.; Cordes, A. W.; Oakley, R. T.; Preuss, K. E.; Reed, R. W. *Chem. Mater.* **1999**, *11*, 164. (j) Barclay, T. M.; Burgess, I. J.; Cordes, A. W.; Oakley, R. T.; Reed, R. W. *J. Chem. Soc., Chem. Comm.* **1998**, 1939. (k) Britten, J. F.; Cordes, A. W.; Haddon, R. C.; Itkis, M. E.; Oakley, R. T.; Reed, R. W.; Robertson, C. M. *CrystEngComm* **2002**, *4*, 205.

(5) (a) Ernest, I.; Holick, W.; Rihs, G.; Schomburg, D.; Shoham, G.; Wenkert, D.; Woodward, R. B. *J. Am. Chem. Soc.* **1981**, *103*, 1540. (b) Boeré, R. T.; Moock, K. H.; Derrick, S.; Hoogerdijk, W.; Preuss, K.; Yip, J. *Can. J. Chem.* **1993**, *71*, 473. (c) Parvez, M.; Boeré, R. T.; Derrick, S.; Moock, K. H. *Acta Crystallogr., Sect. C* **1995**, *51*, 2116. (d) Bond, A. D.; Haynes, D. A.; Rawson, J. M. *Can. J. Chem.* **2002**, *80*, 1507. (e) Amin, M.; Rees, C. W. *J. Chem. Soc., Perkin Trans. 1* **1989**, 2495. (f) Amin, M.; Rees, C. *J. Chem. Soc., Chem. Commun.* **1989**, 1137. (g) Scholz, U.; Roesky, H. W.; Schimkowiak, J.; Noltemeyer, M. *Chem. Ber.* **1989**, *122*, 1067.

(6) (a) Burford, N.; Chivers, T.; Richardson, J. F. *Inorg. Chem.* **1983**, *22*, 1482. (b) Burford, N.; Chivers, T.; Codding, P. W.; Oakley, R. T. *Inorg. Chem.* **1982**, *21*, 982. (c) Chivers, T.; Edwards, M.; Parvez, M. *Inorg. Chem.* **1992**, *31*, 1861. (d) Chivers, T.; Dhathathreyan, K. S.; Liblong, S. W.; Parks, T. *Inorg. Chem.* **1988**, *27*, 1305. (e) Chivers, T.; Doxsee, D. D.; Hilts, R. W. *Inorganic Experiments*, 2nd ed; Woollins, J. D., Ed; Wiley-VCH: Weinheim, Germany, 2003; p 287. (f) Jolly, W. L. *The Synthesis and Characterization of Inorganic Compounds*; Prentice Hall: Englewood Cliffs, NJ, 1970; p 484.

(7) (a) Boeré, R. T.; Cordes, A. W.; Oakley, R. T.; Reed, R. W. *J. Chem. Soc., Chem. Commun.* **1985**, 655. (b) Boeré, R. T.; Cordes, A. W.; Craig, S. L.; Oakley, R. T.; Reed, R. W. *J. Am. Chem. Soc.* **1987**, *109*, 868. (c) Oakley, R. T. *Can. J. Chem.* **1984**, *62*, 2763. (d) Pascal, R. A.; L'Esperance, R. P. *J. Am. Chem. Soc.* **1994**, *116*, 5167.

(8) (a) Burford, N.; Chivers, T.; Rao, M. N. S.; Richardson, J. F.; *Inorg. Chem.* **1984**, *23*, 1946. (b) Chivers, T.; Dhathathreyan, K. S.; Ziegler, T. *J. Chem. Soc., Chem. Commun.* **1989**, 86. (c) Chivers, T.; Edwards, M.; Meetsma, A.; van de Grampel, J. D.; van der Lee, A. *Inorg. Chem.* **1992**, *31*, 2156. (d) Chivers, T.; Hilts, R. W.; Parvez, M.; Ristic-Petrovic, D.; Hoffman, K. *J. Organomet. Chem.* **1994**, *480*, C4. (e) Chivers, T.; Hilts, R. W.; Parvez, M.; Ristic-Petrovic, D. *Can. J. Chem.* **1995**, *73*, 1380.

(9) (a) Chivers, T.; Edwards, M.; Gao, X.; Hilts, R. W.; Parvez, M.; Vollmerhaus, R. *Inorg. Chem.* **1995**, *34*, 5037. (b) Brock, M.; Chivers, T.; Parvez, M.; Vollmerhaus, R. *Inorg. Chem.* **1997**, *36*, 485. (c) Chivers, T.; Cowie, M.; Edwards, M.; Hilts, R. W. *Inorg. Chem.* **1992**, *31*, 3349. (d) Chivers, T.; Gao, X.; Parvez, M. *Inorg. Chem.* **1995**, *34*, 1681. (e) Vollmerhaus, R.; Hilts, R. W.; Parvez, M.; Gao, X. L.; Chivers, T. *Phosphorus, Sulfur Silicon Related Elem.* **1994**, *93*, 425. (f) Hilts, R. W.; Gao, X. L.; Parvez, M.; Chivers, T. *Phosphorus, Sulfur Silicon Related Elem.* **1994**, *93*, 431. (g) Chivers, T.; Gao, X. L.; Hilts, R. W.; Parvez, M.; Vollmerhaus, R. *Inorg. Chem.* **1995**, *34*, 1180. (h) Chivers, T.; Hilts, R. W. *Coord. Chem. Rev.* **1994**, *137*, 201. (i) Chivers, T.; Hilts, R. W.; Parvez, M.; Vollmerhaus, R. *Inorg. Chem.* **1994**, *33*, 3459. (j) Chivers, T.; Edwards, M.; Hilts, R. W.; Parvez, M.; Vollmerhaus, R. *Inorg. Chem.* **1994**, *33*, 1440. (k) Chivers, T.; Edwards, M.; Meetsma, A.; van de Grampel, J. C. *Inorg. Chem.* **1992**, *31*, 2156.

of the dianion $\mathbf{4}^{2-}$ exists when generated chemically by superhydride reduction of **4** in THF solution.[9]

In an effort to further identify and characterize their redox processes, we now report results from a detailed voltammetric and in situ EPR[10] spectroelectrochemical study on these compounds. While there is a long history of electrolysis inside an EPR resonant cavity,[11] electrochemists have more recently developed the concept of simultaneous electrochemical EPR spectroscopy (SEEPR)[12] by improving cell designs so that cyclic voltammograms can be measured in electrolysis cells within EPR resonant cavities with a minimum of distortion.[13] Neudeck and Kress have even shown that real-time EPR spectroscopy obtained during the course of a cyclic voltammetric potential scan is possible.[14] In this paper, we report for the first time the spectroelectrochemical detection of the radical anions $\mathbf{1}^{\bullet-}-\mathbf{4}^{\bullet-}$ by in situ electrolysis employing a modified version of the working electrode first described by Neudeck and Kress. The assignment of the characteristic EPR spectra of the radical monoanions to planar or folded heterocyclic structures has been attempted using UB3LYP/6-31G(d) calculations. Rate constants for the apparent first-order decay of all the radical anions were determined from SEEPR data; rate constants were also determined from the cyclic voltammetric responses of compounds **1c** and **3**; possible chemical mechanisms for the decay of these species are discussed.

Experimental Section

Reagents and General Procedures. The heterocycles (see Chart 1) were prepared by the literature methods: **1a**−**f**,[5b] **2**,[15] **3**,[5a] and **4**.[6e] Dichloromethane and acetonitrile (BDH, reagent grade) were purified by distillation (CH_3CN, first over P_2O_5, then CaH_2; CH_2Cl_2, over CaH_2). Both solvents were purged with dry nitrogen prior to use. Electrochemical grade tetrabutylammonium hexafluorophosphate [^{n}Bu$_4$N][PF_6] (Fluka) was used as the supporting electrolyte and was kept in a desiccator/glovebox prior to use. Hexaammineruthenium(III) chloride (Aldrich) and 1,1-diphenyl-2-picryl-hydrazyl (DPPH) (Aldrich) were stored in a refrigerator prior to use. Ferrocene, prepared following the procedure described by Jolly,[6f] was sublimed prior to use.

Voltammetry. Cyclic voltammograms (CVs) were obtained at temperatures between 0 and 22 °C in both acetonitrile and dichloromethane solutions containing 0.1 and 0.4 M [^{n}Bu$_4$N][PF_6], respectively, as the supporting electrolyte. These solutions were purged with dry nitrogen for 10 min directly before use, and a blanket of nitrogen gas covered the solution during all experiments. The CVs were executed using a BioAnalytical Systems CV-50 computer-controlled potentiostat. The cell design utilized a conventional three-electrode setup with a 3.0 mm diameter glassy-carbon (GC) working electrode, a platinum-wire auxiliary, and a silver-wire quasi-reference electrode. The reference electrode was separated from the bulk solution by a fine-porosity frit. Initial background scans characterized the size of the electrochemical window and provided an estimate of the likely background current. The CVs were obtained over scan rates of 0.050−20 V s^{-1}. All potentials are reported vs the operative formal potential, $E^{0/}_{Fc^{+/0}}$, for the Fc^+/Fc redox couple (Fc = ferrocene), which was used as an internal standard. The GC working electrode area (5.4×10^{-2} cm^2) was determined from the peak current value obtained for the reversible one-electron reduction of hexaammineruthenium(III) chloride (1.0 mM, 2.0 mM, and 3.0 mM solutions) in water (0.5 M KCl) under conditions of cyclic voltammetry and using the Randles−Sevcik equation.[16]

$$I_p = 0.4463nF\left(\frac{nF}{RT}\right)^{1/2}AD^{1/2}\nu^{1/2}C \qquad (1)$$

where I_p is the peak current (A), n (the number of electrons in the charge-transfer process) is taken to be 1.0, A is the electrode area (cm^2), D is the diffusion coefficient (taken to be 9.1×10^{-6} cm^2 s^{-1}),[17] C is the concentration (mol cm^{-3}), ν is the scan rate (V s^{-1}), and the other symbols have their usual meanings. The electrode was polished with 0.3 micron alumina on a clean polishing cloth (Buehler, USA), rinsed with distilled water, and dried with tissue paper prior to use. Linear plots of I_p vs $\nu^{1/2}$ were obtained for the reduction process of both **1c** and **3** in CH_2Cl_2, suggesting that mass transport is diffusion controlled; direct application of the Randles−Sevcik equation led to estimates of the diffusion coefficients (D) for **1c** and **3**.[18]

Simulations of the Cyclic Voltammetric Responses for 1c and 3. Simulations of cyclic voltammetric responses for **1c** and **3** were executed using *DigiSim* (version 3.05).[19] The primary objective was to confirm that the postulated "EC" mechanism (A + e ⇌ B; B → C (k_f)) was a satisfactory explanation for the disappearance of the radical anion and to determine the value of the rate constant k_f.

(10) Selected abbreviations: EPR, electron paramagnetic resonance; ESR, electron spin resonance; CV, cyclic voltammetry; hfc, hyperfine coupling; UV-PES, ultraviolet photoelectron spectroscopy.

(11) (a) Maki, A. H.; Geske, D. H. *J. Chem. Phys.* **1959**, *30*, 1356. (b) Geske, D. H.; Maki, A H. *J. Am. Chem. Soc.* **1960**, *82*, 2671. (c) Fritz, H. P; Artes, R. O. *Electrochim. Acta* **1981**, *26*, 417. (d) Adams, R. N. *J. Electroanal. Chem.* **1964**, *8*, 151. (e) Geske, D. H.; Ragle, J. L. *J. Am. Chem. Soc.* **1961**, *83*, 3532. (f) Piette, L. H.; Ludwig, R.; Adams, R. N. *Anal. Chem.* **1962**, *34*, 916. (g) Piette, L. H.; Ludwig, R.; Adams, R. N. *J. Am. Chem. Soc.* **1962**, *84*, 4212. (h) Yokoyama, M.; Satoh, T.; Ohya-Nishiguchi, H.; Kamada, H.; Kasai, N.; Matsue, T. *Chem. Lett.* **1995**, 919. (i) Bagchi, R. N.; Bond, A. M.; Scholz, F. *Electroanalysis* **1989**, *1*, 1. (j) Webster, R. D.; Bond, A. M.; Coles, B. A.; Compton, R. G. *J. Electroanal. Chem.* **1996**, *404*, 303. (k) Waller, A. M.; Compton, R. G. *Comp. Chem. Kinetics* **1989**, *29*, 297. (l) Goldberg, I. B.; McKinney, T. M. *Laboratory Techniques in Electroanalytical Chemistry*; Marcel Dekker: New York, 1984; p 675. (m) Allendoerfer, R. D.; Martinchek, G. A.; Bruckenstein, S. *Anal. Chem.* **1975**, *47*, 890. (n) Goldberg, I. B.; Bard, A. J. *Magnetic Resonance in Chemistry and Biology*; Marcel Dekker: New York, 1975; p 255. (o) Compton, R. G.; Waller, A. M. *J. Electroanal. Chem.* **1985**, *195*, 289. (p) Allendoerfer, R. D.; Carroll, J. B., Jr. *J. Mag. Res.* **1980**, *37*, 497. (q) Levy, D. H.; Myers, R. J. *J. Chem. Phys.* **1964**, *41*, 1062. (r) Ohya-Nishiguchi, H. *Bull. Chem. Soc. Jpn.* **1979**, *52*, 2064. (s) Goldberg, I. B.; Bard, A. J. *J. Phys. Chem.* **1971**, *75*, 3281. (t) Meinzer, R. A.; Pratt, D. W.; Myers, R. J. *J. Am. Chem. Soc.* **1969**, *91*, 6623. (u) Williford, J. D.; VanReet, R. E.; Eastman, M. P.; Prater, K. B. *J. Electrochem. Soc.* **1973**, *120*, 1498.

(12) Because of the common interchangeable usage of EPR and ESR, the acronym SEESR has also appeared in the literature.

(13) (a) Webster, R. D.; Bond, A. M.; Coles, B. A.; Compton, R. G. *J. Electroanal. Chem.* **1996**, *404*, 303. (b) Fiedler, D. A.; Koppenol, M.; Bond, A. M. *J. Electrochem. Soc.* **1995**, *142*, 862.

(14) Neudeck, A.; Kress, L. *J. Electroanal. Chem.* **1997**, *437*, 141.

(15) Gleiter, R.; Bartetzko, R.; Cremer, D. *J. Am. Chem. Soc.* **1984**, *106*, 3437.

(16) Bard, A. J.; Faulkner, L. R. *Electrochemical Methods: Fundamentals and Applications*, 2nd ed.; Wiley: New York, 2001.

(17) Marken, F.; Eklund, J. C.; Compton, R. G. *J. Electroanal. Chem.* **1995**, *395*, 335.

(18) Estimates of the diffusion coefficients (D) for compounds **1c** (D = 1.94 (±0.1) × 10^{-5} cm^2 s^{-1}) and **3** (D = 1.96 (±0.1) × 10^{-5} cm^2 s^{-1}) were determined from their cyclic voltammograms in CH_2Cl_2 by application of eq 1, using the assumption that $RTk_f/F\nu$ < 0.1 over scan rates of 0.1−0.6 V s^{-1}.

(19) *DigiSim for Windows 95*, version 3.05; Bioanalytical Systems, Inc.: West Lafayette, IN, 2000.

Nicholson and Shain's graphical method of evaluating k_f was unsatisfactory since the influence of uncompensated resistance had not been considered.[20]

In Situ EPR Electrochemistry. In situ EPR electrochemistry experiments were conducted using a Wilmad WG-810 quartz electrolytic flat cell with a gold-micromesh working electrode,[14] a platinum-wire auxiliary, and a copper-wire quasi-reference electrode. This cell was situated inside a Bruker EMX 113 spectrometer operating at X-band frequencies (9.8 GHz) at 18 ± 2 °C. Initially, the CVs were obtained in a conventional cell using an EG&G 263A potentiostat to confirm the viability of the analyte solutions via reference to the previous voltammetric measurements. Then a modified Schlenk tube holding the previously dried flat cell and copper reference electrode was evacuated and refilled with argon. Approximately 2 mL of the analyte solution was syringed out of the primary cell and injected into the flat cell with rigorous exclusion of air and moisture. The platinum-wire auxiliary and gold-mesh working electrodes were then inserted, thereby forming a seal for the cell to prevent contamination. The electrochemical cell was then inserted into the EPR cavity and connected to the potentiostat via nonmagnetic leads. The CV studies were then applied to determine the exact potential for the reduction process versus the reference electrode in this cell, and controlled potential electrolysis experiments were carried out with the potential set to just beyond (approximately −0.01 V) the cathodic peak potential. The EPR spectra were monitored in intensity-versus-time mode after electrolysis was terminated. Plots of $\ln(C_t/C_{t=0})$ vs t (where C = signal intensity, t = time in seconds) as well as of $1/(C_t/C_{t=0})$ vs t were used to determine the rate of decay of the radicals. Results from a limited number of repeat measurements for compounds **1a**−**f** were undertaken and led to an error estimate in k_f values of approximately ±0.02 s^{-1}. Simulations of EPR spectra were performed with Bruker *SimFonia* (version 1.25) and *WinSim* (version 0.98, 2002) software.[21] Experimental g values were determined with reference to external, solid DPPH (2.0037 ± 0.0002).[22] Spectral parameters for compounds **1**−**3** in CH_2Cl_2: conversion times = 40.96 or 81.92 s, sweep width = 6.0 mT, modulation amplitude = 0.01 mT. Compound **4**: conversion time = 40.96 s, modulation amplitude = 0.1 mT, sweep width = 8.0 mT (in CH_2Cl_2), 10.0 mT (in CH_3CN).

Computational Details. Full geometry optimizations were performed at the B3LYP/6-31G(d) (neutral) and UB3LYP/6-31G(d) (anion) levels of theory for both planar and bent conformations for *all* the molecules and radicals in this study. The structures of neutral **1**−**4** were first optimized at the PM3 semiempirical level in *HyperChem 5.1*[23] and then transferred into the *Gaussian 98* program package for the density functional theory (DFT) calculations.[24] The structures of the radical anions were obtained after starting from the DFT-optimized neutral molecule geometries. The results of the frequency calculations were used to correct the zero-point energies of all species. Nonrelativistic hfc constants were calculated for the radical anions in both conformations using the unrestricted Kohn−Sham formalism, employing the same basis sets and density functional used for the geometry optimizations.

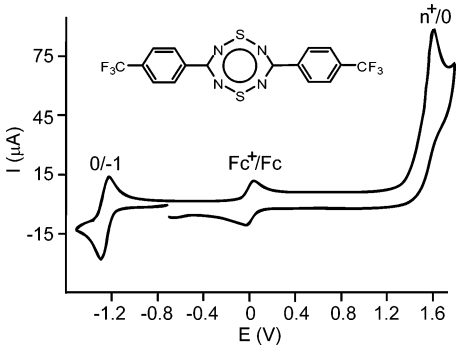

Figure 2. Cyclic voltammogram of 0.9 mM **1e** and 0.6 mM Fc in CH_3CN at a GC electrode at 22 °C, 0.1 M [^{n}Bu$_4$N][PF$_6$], ν = 0.2 V s^{-1}.

Table 1. Summary of Cyclic Voltammetric Data for **1**−**4** Obtained at a GC Electrode, Area = 0.054 cm^2 at ν = 0.2 V s^{-1} and T = 22 °C[e]

cmpd	conc (mM)	E_p^{a1} (V)	E_p^{c1} (V)	$E_m \cong E^{0/}$ (V)[a]	ΔE_{pp} (V)[b]	E_p^{a2} (V)	ΔE_{ox-red} (V)[c]
CH_3CN solutions with 0.1 M [^{n}Bu$_4$N][PF$_6$] supporting electrolyte							
1a	0.1	−1.310	−1.366	−1.338	0.056	1.123	2.463
1b	0.3	−1.306	−1.370	−1.338	0.064	1.310	2.648
1c	0.1	−1.293	−1.355	−1.324	0.062	1.457	2.781
1d	0.1	−1.253	−1.309	−1.281	0.056	1.491	2.774
1e	0.9	−1.229	−1.299	−1.264	0.070	1.603	2.867
1f	0.3	−1.220	−1.288	−1.254	0.067	1.567	2.821
2	1.0	−1.415	−1.497	−1.456	0.082	1.513	2.969
3	0.9	−1.687	−1.759	−1.723	0.072	0.963	2.686
4	2.0	−1.613	−1.813	−1.713	0.200	0.713	2.426
CH_2Cl_2 solutions with 0.4 M [^{n}Bu$_4$N][PF$_6$] supporting electrolyte							
1c	2.8	−1.332	−1.454	−1.393	0.122	1.516	2.909
3	2.7	−1.712	−1.828	−1.770	0.116	0.900	2.670
4	3.4		−1.877			0.657	2.534[d]

[a] $E_m = [E_p^{a1} + E_p^{c1}]/2 \approx E^{0/}$. [b] $\Delta E_{pp} = E_p^{a1} - E_p^{c1}$. [c] $\Delta E_{ox-red} = E_p^{a2} - E_m$. [d] $\Delta E_{ox-red} = E_p^{a2} - E_p^{c2}$. [e] All potentials are vs $E^{0/}_{Fc^{+/0}}$.

Results

Voltammetry. A representative CV of compound **1e** in CH_3CN (including the internal Fc reference) is shown in Figure 2. All potential data are given with respect to $E^{0/}_{Fc^{+/0}}$, the formal potential for the Fc^+/Fc redox couple. Data for the cyclic voltammetric responses for compounds **1a**−**1f** and **2**−**4** in CH_3CN and **1c**, **3**, and **4** in CH_2Cl_2 are reported in Table 1 for a scan rate of 0.2 V s^{-1}. Estimates of the formal potentials, $E^{0/}$, for the one-electron transfers occurring over the potential range of ∼ −1.25 to ∼ −1.77 V vs $E^{0/}_{Fc^{+/0}}$ (see Figure 2) were obtained by averaging the corresponding cathodic and anodic peak potentials, E_p^{c1} and E_p^{a1}, to obtain the "midpoint" potential, E_m, which is assumed to be a good approximation of the standard potential, $E^{0/}$. With the exception of compound **4**, the instability of the reduction product, which will be discussed in detail later for compounds **1c** and **3** in CH_2Cl_2, has no significant impact on

(20) (a) Nicholson, R. S.; Shain, I. *Anal. Chem.* **1964**, *36*, 706. (b) Nicholson, R. S. *Anal. Chem.* **1966**, *38*, 1406.
(21) Duling, D. R. *J. Mag. Res., Ser. B* **1994**, *104*, 105.
(22) Weil, J. A.; Bolton, J. R.; Wertz, J. E. *Electron Paramagnetic Resonance*; John Wiley & Sons: New York, 1994.
(23) *HyperChem*, version 5.11; Hypercube, Inc.: Gainesville, FL,1999.
(24) Frisch, M. J.; Trucks, G. W.; Schlegel, H. B.; Scuseria, G. E.; Robb, M. A.; Cheeseman, J. R.; Zakrzewski, V. G.; Montgomery, J. A., Jr.; Stratmann, R. E.; Burant, J. C.; Dapprich, S.; Millam, J. M.; Daniels, A. D.; Kudin, K. N.; Strain, M. C.; Farkas, O.; Tomasi, J.; Barone, V.; Cossi, M.; Cammi, R.; Mennucci, B.; Pomelli, C.; Adamo, C.; Clifford, S.; Ochterski, J.; Petersson, G. A.; Ayala, P. Y.; Cui, Q.; Morokuma, K.; Malick, D. K.; Rabuck, A. D.; Raghavachari, K.; Foresman, J. B.; Cioslowski, J.; Ortiz, J. V.; Stefanov, B. B.; Liu, G.; Liashenko, A.; Piskorz, P.; Komaromi, I.; Gomperts, R.; Martin, R. L.; Fox, D. J.; Keith, T.; Al-Laham, M. A.; Peng, C. Y.; Nanayakkara, A.; Gonzalez, C.; Challacombe, M.; Gill, P. M. W.; Johnson, B.; Chen, W.; Wong, M. W.; Andres, J. L.; Gonzalez, C.; Head-Gordon, M.; Replogle, E. S.; Pople, J. A. Gaussian 98; Gaussian, Inc.: Pittsburgh, PA, 1998.

values of the peak potentials at a scan rate of 0.2 V s^{-1}. The peak potentials (E_p^{a2} values) for the oxidation of the compounds over the potential range ~0.65 to ~1.6 V vs $E^{0/}_{Fc^{+/0}}$ (see Figure 2) are also given in Table 1.

In CH_3CN solutions with [^{n}Bu$_4$N][PF_6] as the supporting electrolyte, all nine compounds gave rise to at least one oxidation and one reduction process, as previously reported from a study in CH_2Cl_2.[5b] The reduction process displayed close to electrochemically reversible behavior for compounds **1a**−**1f, 2**, and **3**, with anodic (E_p^{a1}) to cathodic (E_p^{c1}) peak-to-peak separations ΔE_{pp} in the range of 56−82 mV. However, the anodic peak heights were generally lower than might be expected for a simple reversible charge-transfer process—even at scan rates up to 20 V s^{-1} or upon cooling to 0 °C. This could be caused by the low solubility of these compounds in CH_3CN (<1 mM) and the likely high reactivity of the reduction product with traces of oxygen. For some compounds, additional rigorous purging with nitrogen did effect an increase in the anodic peak current, lending support to this hypothesis. The midpoint potential, E_m, is assumed to be a good estimate of the formal potential, $E^{0/}$. The range of E_m values for compounds **1a**−**f** in CH_3CN is ~0.08 V, comparable to the ~0.12 V observed in CH_2Cl_2,[5b] but larger than that seen for the substituted aryl 1,2,3,5-dithiadiazoles bearing the same para substituents.[25] A small but noticeable trend toward more negative values of E_m for reduction of **1a**−**f** is apparent as the R group is changed from electron-donating to electron-withdrawing. In the case of **3**, when scans were continued in the negative potential direction beyond the initial reduction process, a second, irreversible reduction process was observed at −2.19 V. This process appears to involve a single-electron transfer by comparison of peak current heights with that of the first known one-electron reduction but has not been investigated further.

Compound **4** displayed a much less chemically reversible reduction process than for the other compounds. In this case, at moderate scan rates (0.1 V s^{-1}) no return wave was noted, but upon scanning faster (up to 20 V s^{-1}) and lowering the temperature to 0 °C, a small increase in the relative size of the return wave was observed. The peak potential for the reduction process for **4** occurs at −1.81 V in CH_3CN and −1.88 V in CH_2Cl_2 vs $E^{0/}_{Fc^{+/0}}$ with a GC electrode (ν = 0.2 V s^{-1}). A previous investigation of this system reported the reduction at −1.37 V vs SCE with a Pt electrode in CH_3CN;[9a] on the Fc^+/Fc scale this corresponds approximately to −1.77 V,[26] a value in reasonable agreement with our measured potential in the same solvent. We have not observed a second reduction process for **4** in either CH_3CN or CH_2Cl_2.

The oxidation of **1**−**4** in CH_3CN showed no return waves at any scan rate (0.05−20 V s^{-1}) or temperature (0−22 °C) and is therefore fully irreversible, in the chemical sense, over a wide range of conditions. The anodic peak currents were also much larger than the cathodic peak currents for the corresponding reduction processes, perhaps suggesting that more than one electron is transferred during oxidation (the process occurs near the positive limit of the solvent "window", so catalytic breakdown of the solvent is also a possibility). Compounds **1a** and **3** display a second oxidation process at more positive potentials, possibly associated with oxidation at the methoxy and dimethylamino groups, respectively.

Cyclic voltammetric measurements of compounds **1c** and **3** (representative of the planar and folded structural forms, respectively) focused on quantifying the decay of the reduction product as described by the EC mechanism

$$A + e^- \rightleftharpoons A^{\bullet -} \ (E^{0/}, k_s, \alpha) \qquad (2)$$

$$A^{\bullet -} \rightleftharpoons B \ (K_{eq}, k_f) \qquad (3)$$

where k_s and α are, respectively, the standard heterogeneous rate constant and the transfer coefficient associated with the Butler−Volmer formalism[16] for a heterogeneous electron transfer; K_{eq} and k_f are the equilibrium constant and the rate constant for the follow-up chemical reaction. CH_2Cl_2 was the solvent of choice because of the enhanced solubility of **1c** and **3** (compared with the low (submillimolar) solubility of **1a**−**1f** in CH_3CN, which exacerbated complications caused by background currents and by trace oxygen). Even with the higher concentrations in CH_2Cl_2, background currents were a factor. In the potential regions of interest, these currents are negative and increase more or less linearly with the scan rate, introducing serious errors at scan rates greater than 0.05 V s^{-1}. the use of lower scan rates presented problems associated with adventitious convection. The optimization of simulated CV responses using *DigiSim* was deemed successful when the simulated and experimental peak heights and positions overlaid each other. The adjustable parameters were the apparent $E^{0/}$ as measured vs the silver-wire quasi-reference electrode (see Table 1 for $E^{0/}$ values vs $E^{0/}_{Fc^{+/0}}$), D (assumed to be the same for all species), k_f, and k_s (see eqs 2 and 3). For the purposes of simulation, the value of α (eq 2) was assumed to be 0.5 and the value of K_{eq} (see eq 3) was assumed to be 10^6, rendering the chemical reaction effectively irreversible for the scan rates investigated. The introduction of a background current of -1.0×10^{-6} A (assumed to be constant over the entire voltage range of the CV) effected a decrease in the apparent value of k_f as expected (run no. 5, Table 2). This decrease occurs because the background currents are negative and effect a diminution of the reverse wave, which can easily be misinterpreted as an increase in k_f. The problem is exacerbated with lower concentrations of analyte and/or by higher scan rates. The contribution of capacitive currents is negligible at the scan rate and concentrations investigated. The fit for run no. 2 is shown in Figure 3. The simulated voltammogram for $k_f = 0$ shows that chemical kinetics effect a decrease of $\sim 11 \times 10^{-6}$ A, considerably larger than the -1×10^{-6} to -2×10^{-6} A value observed as background in the relevant potential range. The values of D, k_f, and k_s for **1c** and **3** are not significantly different. The uncertainty of the background

(25) (a) Boeré, R. T.; Moock, K. H. *J. Am. Chem. Soc.* **1995**, *117*, 4755. (b) Boeré, R. T.; Moock, K. H.; Parvez, M. *Z. Anorg. Allg. Chem.* **1994**, 1589.
(26) Connelly, N. G.; Geiger, W. E. *Chem. Rev.* **1996**, *96*, 877.

Table 2. Parameters Used in CV Simulations of **1c** and **3** in CH_2Cl_2 on a GC Electrode at $T = 22$ °C[a]

run no.		c (mM)	v (V/s)	R_u, Ω[a]	$i_{background}$ (A)[b]	D ($cm^2\ s^{-1}$)[c]	k_f (s^{-1})[d]	k_s [e]
1	**1c**	1.05	0.05	320	0	2.58×10^{-5}	0.050	0.04
2	**1c**	2.80	0.05	380	0	2.09×10^{-5}	0.065	0.04
3	**3**	1.10	0.05	320	0	2.3×10^{-5}	0.055	0.015
4	**3**	2.70	0.05	350	0	2.0×10^{-5}	0.06	0.04
5	**3**	2.70	0.05	320	-1.0×10^{-6}	1.85×10^{-5}	0.040	0.04
					estimate of parameter values for **1c** and **3**			
						$2.0 \pm 0.2 \times 10^{-5}$	0.050 ± 0.02	0.04 ± 0.02

[a] R_u values were experimentally measured using the BAS-CV50; a small potential step is applied to the electrode, and the uncompensated resistance R_u is determined from the rate of decay and zero-time intercept of the resultant current transient. [b] $i_{background}$ was included in the simulation only for run no. 5. [c] D values were optimized for each voltammogram. Larger D values for nos. 1 and 3 were effected by the background currents. [d] k_f values were optimized for each voltammogram; the value of K_{eq} (see EC mechanism) was assumed to be 10^6, thereby effecting an essentially irreversible reaction. [e] k_s values were optimized for each voltammogram.

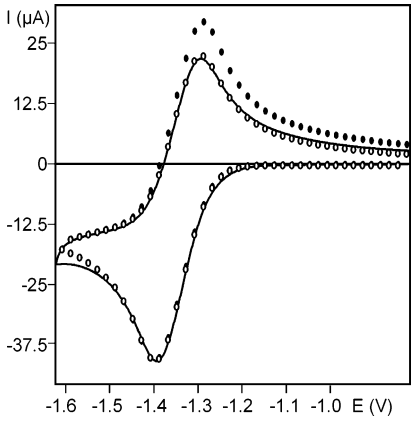

Figure 3. Comparison of an experimental cyclic voltammogram of 2.80 mM **1c** (solid line) at 0.1 V s^{-1} (GC electrode), 0.4 M [^{n}Bu$_4$N][PF_6] in CH_2Cl_2, and a simulated one (○). See Table 2, run no. 2, for simulation parameters. Simulated data for $k_f = 0\ s^{-1}$ is also shown (·).

current on GC suggests a conservative estimate of the uncertainties in the values D, k_f, and k_s (see bottom entry in Table 2). The reasonable agreement of k_f values for two different concentrations of starting material is strong evidence that the decay of $A^{\bullet-}$ is first order. The values of k_s primarily reflect the inadequacy of R_u to account for the observed peak separation, ΔE_{pp}.

EPR Spectroscopy. In situ electrochemical EPR reduction experiments were conducted in CH_2Cl_2 for compounds **1**−**4** as well as in CH_3CN for **1c**,**e**,**f** and **4** with a modified version of the gold-mesh working electrode first described by Neudeck and Kress.[14] For compounds **1**−**3,** reductive electrolysis gave rise to strong EPR signals from single 41 or 82 s scans. Representative spectra from reductive electrolysis of **1c** and **3** are shown in Figure 4 and exhibit high signal-to-noise ratios. The general appearance of the EPR spectra from the reduction of **1a**,**b**,**d**−**f** and **2** is very similar to that of **1c** and is of at least equally high quality. Computer averaging or varying the EPR parameters did not alter the EPR spectra in any significant manner. The broader lines and distorted line shapes associated with **3** find their origin in further hyperfine coupling to both the nitrogen and hydrogen nuclei of the exocylic NMe_2 groups (see the Discussion). In situ EPR electrolysis experiments for **4**, despite the significant chemically irreversible nature of the reduction in CV studies, also produced high-quality EPR data. An example of a 41 s EPR scan obtained during reductive electrolysis of **4**, along with a simulated spectrum,

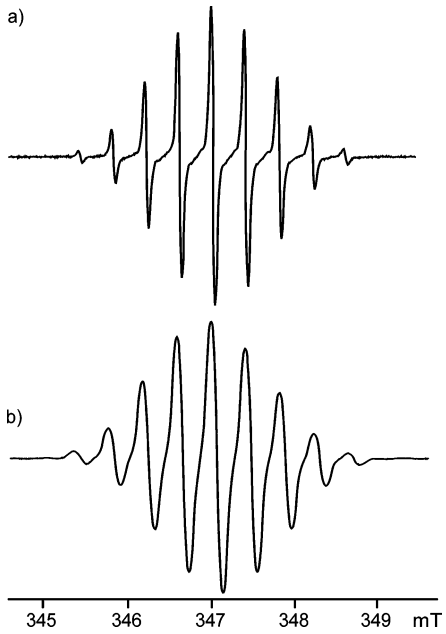

Figure 4. In situ first-derivative EPR spectra obtained during reductive electrolyses (41 s single scans) at a gold-mesh electrode at 18 °C in CH_2Cl_2 (0.4 M [^{n}Bu$_4$N][PF_6]) and modulation frequency 100 kHz of: (a) 6.03 mM solution of compound **1c**, modulation amplitude = 0.01 mT, and (b) 1.21 mM solution of compound **3**, modulation amplitude = 0.03 mT.

is shown in Figure 5. The experimental hfc constants, linewidths, and g values for radicals $\mathbf{1}^{\bullet-}$−$\mathbf{4}^{\bullet-}$, along with the DFT calculated hfc constants, are presented in Table 3. An EPR spectrum of **1c** obtained at high gain with observable satellites in the baseline, along with a simulation including coupling to ^{33}S, ^{13}C, and ^{15}N, is shown in Figure 6.

Kinetic Measurements. Rate constants from the decay of the EPR signals of the radical anions $\mathbf{1}^{\bullet-}$−$\mathbf{4}^{\bullet-}$ in CH_2Cl_2 at 18 ± 2 °C were calculated by electrochemically generating the radical, halting the electrolysis, and measuring the decay of the signal intensity as a function of time at constant field. To minimize the errors associated with material diffusing away from the most sensitive part of the EPR cavity, the spectra were obtained over a moderately short time period (less than 2 min). The slope of plots of $\ln(C_t/C_{t=0})$ vs t (C = signal intensity) (Figure 7) yielded k_f values in the range of 0.02−0.08 for compounds $\mathbf{1}^{\bullet-}$−$\mathbf{3}^{\bullet-}$ and 0.7 for compound $\mathbf{4}^{\bullet-}$, with $t_{1/2}$ values in the range of 1−35 s, assuming first-order kinetics (Table 4). Plots based on second-order kinetics exhibited a much poorer fit to the data.

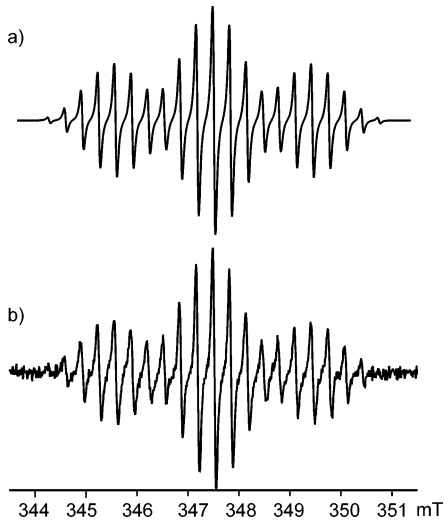

Figure 5. (a) Simulated and (b) experimental first-derivative EPR spectra of **4** obtained during in situ reductive electrolysis (41 s single scan) at a gold-mesh electrode at 18 °C in CH_3CN (0.1 M [^{n}Bu$_4$N][PF_6]), 12.6 mM solution, modulation amplitude = 0.1 mT.

The values of k_f obtained via EPR measurements are compared with those generated from digital simulations (Table 4). The rates obtained by two dramatically different experimental protocols are satisfyingly comparable.

DFT Calculations. The structural dichotomy that exists between compounds **1** and **2** and **3** and **4** has long been of interest to theoreticians.[7,15,27] Improvements in DFT methods and increased computational speed over the past decade have made it possible to calculate hfc constants for main-group elements that are in relatively good agreement with experimental evidence. Various ab initio and DFT methods have recently been explored in determining accurate molecular geometries and isotropic hfc constants for several heterocyclic C,N,S and binary S,N radicals. The UB3LYP functional was employed in each case, in conjunction with 6-31G(d),[28] EPR-III, cc-PVQZ,[29] TZVP,[29,30] or (aug)cc-PVTZ[31] basis sets, with only small differences in the reliability among the different choices as compared to either experimental values or post-Hartree−Fock computational methods.[30] Due to the large size of our systems, we have restricted our calculations to the B3LYP/6-31G(d) (neutral) and UB3LYP/6-31G(d) (anion) methods. For all the molecules, the calculated geometries of both neutral and anion in the respective planar (**1**, **1**$^{\bullet-}$, **2**, **2**$^{\bullet-}$) or folded (**3**, **3**$^{\bullet-}$, **4**, **4**$^{\bullet-}$) geometries were established to be local minima on the potential energy surface through full frequency calculations. The alternative folded structures of **1** and **1**$^{\bullet-}$ and **2** and **2**$^{\bullet-}$ were similarly shown to be true local minima, but the planar forms of **3** and **3**$^{\bullet-}$ and **4** and **4**$^{\bullet-}$ displayed several imaginary frequencies suggestive of saddle points between two degenerate folded ground states. It has been shown previously that **3** has a very strong preference for the folded structure as a consequence of a second-order Jahn−Teller distortion.[2] Calculated structural parameters for the neutral compounds demonstrate good agreement with available crystallographic data (Supporting Information, Table S1).

A comparative table of calculated bond lengths and angles for the radical anions, along with the neutral molecules based on their known starting geometries, is available (Supporting Information, Table S4). Both the planar and folded geometry-optimized conformations of the radical anion **1c** are shown in Figure 8. An increase in the calculated S−N distance is seen for the planar conformation of the radical anions of **1** and **2** (∼0.06 Å) when compared with the planar neutral calculated geometries, while the C−N bond length remains relatively unchanged, and the N−C−N bond angle widens by ∼5°. These structural changes are all consistent with the

Table 3. Experimental and DFT Calculated EPR Data for Free Radicals **1**$^{\bullet-}$−**4**$^{\bullet-}$ [a]

compd	g value[b]	line width (mT)	nucleus	expt hfc (mT)	calcd hfc (mT) (planar)[c]	calcd hfc (mT) (folded)[c]
1a$^{\bullet-}$	2.0087	0.042	$^{14}N_{1-4}$	0.400	0.372	0.385
			^{33}S		0.505	0.554
			^{13}C		0.606	0.472
1b$^{\bullet-}$	2.0087	0.044	$^{14}N_{1-4}$	0.399	0.372	0.381
			^{33}S		0.506	0.537
			^{13}C		0.605	0.477
1c$^{\bullet-}$	2.0087	0.038	$^{14}N_{1-4}$	0.398	0.372	0.380
		0.033[d]		0.396[d]	0.372	0.380
			^{33}S		0.507	0.531
			^{13}C		0.605	0.478
1d$^{\bullet-}$	2.0087	0.036	$^{14}N_{1-4}$	0.396	0.370	0.377
			^{33}S		0.511	0.529
			^{13}C		0.602	0.478
1e$^{\bullet-}$	2.0087	0.041	$^{14}N_{1-4}$	0.390	0.369	0.378
		0.053[e]		0.388[e]	0.369	0.378
			^{33}S		0.514	0.530
			^{13}C		0.598	0.472
1f$^{\bullet-}$	2.0087	0.039	$^{14}N_{1-4}$	0.391	0.368	0.372
		0.040[f]		0.388[f]	0.368	0.372
			^{33}S		0.512	0.521
			^{13}C		0.599	0.480
2$^{\bullet-}$	2.0094	0.042	$^{14}N_{1-4}$	0.405	0.374	0.411
			^{33}S		0.495	0.578
			^{13}C		0.624	0.469
3$^{\bullet-}$	2.0084	0.034[g]	$^{14}N_{1-4}$	0.409[g]	0.385	0.437
			$^{14}N_{exo}$	0.042[g]	0.048	0.079
			$^{1}H_{exo}$	0.011	0.033	0.009
			^{33}S		0.503	0.691
			^{13}C		0.590	0.401
4$^{\bullet-}$	2.0065	0.055[h]	$^{14}N_{1-4}$	0.326[h]	0.158	0.343
			$^{31}P_{1,2}$	1.923[h]	1.396	2.247
		0.040[i]	$^{14}N_{1-4}$	0.330[i]	0.158	0.343
			$^{31}P_{1,2}$	1.961[i]	1.396	2.247
			^{33}S		0.503	0.718

[a] In CH_2Cl_2 at mod. amp. = 0.01 mT, T = 18 °C, single 41 s scan. [b] Referenced versus DPPH (g = 2.0037 ± 0.0002).[22] [c] Gas-phase values from UB3LYP/6-31G(d) calculations (see text). [d] In CH_3CN at mod. amp. = 0.02 mT, T = 18 °C, single 82 s scan. [e] In CH_3CN at mod. amp. = 0.1 mT, T = 18 °C, single 82 s scan. [f] In CH_3CN at mod. amp. = 0.05 mT, T = 18 °C, single 82 s scan. [g] In CH_2Cl_2 at mod. amp. = 0.03 mT, T = 18 °C, single 41 s scan. [h] In CH_2Cl_2 at mod. amp. = 0.1 mT, T = 18 °C, single 41 s scan. [i] In CH_3CN at mod. amp. = 0.1 mT, T = 18 °C, single 41 s scan.

(27) (a) Millefiori, S.; Millefiori, A. *Inorg. Chim. Acta* **1984**, *90*, L55. (b) Boutique, J. P.; Riga, J.; Verbist, J. J.; Delhalle, J.; Fripiat, J. G.; Haddon, R. C.; Kaplan, M. L. *J. Am. Chem. Soc.* **1984**, *106*, 312.
(28) (a) Kaszynski, P. *J. Phys. Chem. A* **2001**, *105*, 7615. (b) Kaszynski, P. *J. Phys. Chem. A* **2001**, *105*, 7626.
(29) (a) Hermosilla, L.; Calle, P.; García de la Vega, J. M.; Seiro, C. *J. Phys. Chem. A* **2005**, *109*, 1114. (b) Hermosilla, L.; Calle, P.; García de la Vega, J. M.; Seiro, C. *J. Phys. Chem. A* **2005**, *109*, 7626.
(30) Gassman, J.; Fabian, J. *Mag. Res. Chem.* **1996**, *34*, 913.
(31) Boeré, R. T.; Tuononen, H. M.; Chivers, T.; Roemmele, T. L. *J. Organomet. Chem.* **2007**, *692*, 2683.

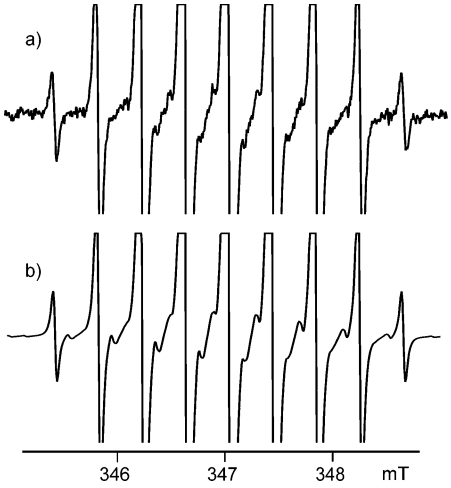

Figure 6. (a) In situ first-derivative EPR spectrum of **1c**$^{\bullet-}$ in CH_3CN (0.1 M [^{n}Bu$_4$N][PF$_6$]), modulation frequency 100 kHz, modulation amplitude = 0.02 mT shown at very high gain, and (b) simulated EPR spectrum including coupling to ^{33}S at 0.530 mT, ^{13}C at 0.550 mT, and ^{15}N at 0.558 mT, line width = 0.037 mT.

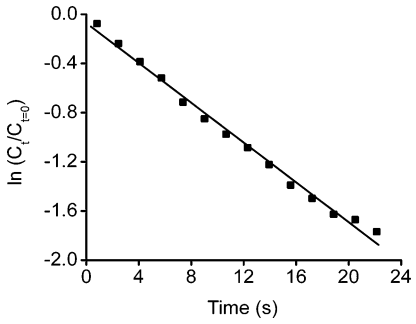

Figure 7. Plot of ln($C_t/C_{t=0}$) ($C_{t=0}$ = signal intensity at time t = 0 s and C_t = signal intensity at time t) vs t (s) measured by a time-sweep EPR experiment during the decay of a radical obtained by the reductive electrolysis of **1c** in CH_2Cl_2 at 18 (±2) °C. Slope = −0.08, R = 0.993.

Table 4. Experimentally Determined Rate Constants and Corresponding Half-Lives for **1**$^{\bullet-}$−**4**$^{\bullet-}$

	k_f (s^{-1})		$\tau_{1/2}$ (s) = ln[2]/k_f	
compound	SEEPR[a]	Sim[b]	SEEPR[c]	Sim[c]
1a$^{\bullet-}$	0.04		17	
1b$^{\bullet-}$	0.02		35	
1c$^{\bullet-}$	0.08	0.05 ± 0.02	9	14 ± 5
1d$^{\bullet-}$	0.05		14	
1e$^{\bullet-}$	0.05		14	
1f$^{\bullet-}$	0.07		10	
2$^{\bullet-}$	0.02		35	
3$^{\bullet-}$	0.05	0.05 ± 0.02	14	14 ± 5
4$^{\bullet-}$	0.7		1	

[a] Extracted from the graphical analysis obtained by time-sweep EPR experiments at 18 (±2) °C in CH_2Cl_2. Error ± 0.02 s^{-1} (see the Experimental Section). [b] Determined from fits to CV data obtained in CH_2Cl_2 at T = 22 °C using *DigiSim*. No significant difference could be discerned for the k_f values of **1c** and **3** (see Table 2 and related discussion). [c] Computed from corresponding k_f values.

population of the π^* LUMO of the neutral molecule (Figure 1b). For the folded compounds **3** and **4**, the S−N bond distance is also seen to elongate in the anion by ∼0.05 Å, while the N−C−N angle opens up by 8° (**3**$^{\bullet-}$) and 12° (**4**$^{\bullet-}$), respectively. The transannular S···S distances show a substantial increase of 0.31 Å for **3**$^{\bullet-}$ and 0.48 Å for **4**$^{\bullet-}$.

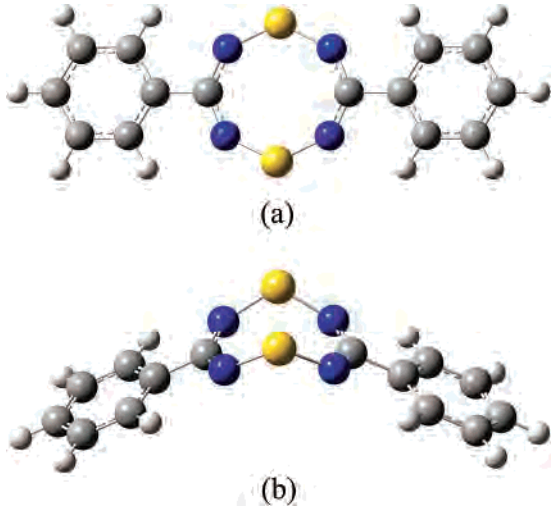

Figure 8. UB3LYP/6-31G(d) geometry optimized structures for the radical anion of **1c** in the (a) planar (as found in the neutral species) and (b) alternative folded conformation.

Discussion

EPR Spectroscopic Characterization of Radical Anions. The spectra from the in situ electrochemical EPR experiments are, in all cases, consistent with the generation of the dithiatetrazocine radical anions **1**$^{\bullet-}$−**4**$^{\bullet-}$. The radicals so formed are transient and decay quickly upon termination of electrolysis. Using isotropic EPR simulation software (see Experimental Section), we were able to obtain simulated EPR spectra that exhibit line positions and line shapes that agree well with values deduced from the experimental spectra. For **1**$^{\bullet-}$ and **2**$^{\bullet-}$, good agreement could be obtained for hfc to four equivalent ^{14}N using Lorentzian line shapes. There is thus no experimental evidence for spin delocalization onto the exocylic substituents in these examples. The DFT calculations indicate that hfc to the sulfur and ring carbon atoms is expected to be of similar magnitude to the coupling to nitrogen (see below). Since the singly occupied molecular orbital (SOMO) is nodal at the ring carbon atoms, hfc to these ^{13}C nuclei is a consequence of spin polarization, and the large size of the calculated coupling constant is a reflection of the larger nuclear g value of C compared with that of the other nuclei (1.405/0.429/0.404 for C/S/N) and not to a high spin density at C.

A small but consistent trend in the size of the experimental ^{14}N hfc is observed for compounds **1a**−**f**$^{\bullet-}$ following the expected inductive influences of the aryl ring substituents. Thus, the hfc values decrease slightly (from 0.400 to 0.388 mT) as the substituents change from electron-donating to electron-withdrawing. A small but distinct influence also occurs in the reversible potentials for reduction (see below), and both are consistent with substituent effects on the electronic properties of the redox orbital, the LUMO of **1** (Figure 1b), or the SOMO of **1**$^{\bullet-}$. Consistent with this interpretation, the stronger donating properties of directly bound *tert*-butyl (**2**$^{\bullet-}$) and dimethylamino (**3**$^{\bullet-}$) groups induce significantly larger hfc to the ring ^{14}N nuclei.

The broader lines and more complex line shapes in the EPR spectrum of **3**$^{\bullet-}$ both indicate the presence of unresolved

hfc; a good simulation was obtained by incorporating 0.042 mT coupling to the two exocyclic dimethylamino ^{14}N atoms. But the best line shape match using strictly Lorentzian functions required the further inclusion of hfc to the 12 protons on the exocylic methyl groups of 0.011 mT, leading to a line width of 0.34 mT that is in good agreement with the value for the other radicals. In situ electrochemical EPR attempts to detect the radical anions of **1** were also made in CH_3CN but were pursued only in the case of **1c**,**e**,**f**, which are the more soluble species in this solvent (but see below under Structures of the Radical Anions).

The high level of chemical irreversibility associated with the reduction of **4** suggested that the suitability of this system in SEEPR experiments would be limited.[13a,32] However, the EPR signal obtained from this electrolysis experiment conclusively identified the formation of a transient radical anion $\mathbf{4}^{\bullet-}$. The signal-to-noise ratio is poorer than that detected for $\mathbf{1}^{\bullet-}$−$\mathbf{3}^{\bullet-}$, which is attributable to a combination of the shorter half-life of $\mathbf{4}^{\bullet-}$, the wider sweep window required for the measurement, and the distribution of the signal intensity over 3 times as many lines; nevertheless, an excellent simulation of the experimental spectrum is obtained by allowing for coupling of the unpaired electron with two ^{31}P nuclei ($I = {}^1/_2$, 100%), producing a 1:2:1 triplet (a_P = 1.923 mT), which is further split into 1:4:10:16:19:16:10:4:1 nonets due to coupling to the four equivalent ^{14}N nuclei (a_N = 0.326 mT). While we cannot be certain that $\mathbf{4}^{\bullet-}$ is the direct product of a one-electron reduction of **4**, this seems highly likely on the basis of comparison with the results obtained on C,N,S analogues **1**−**3**. Our ability to detect this very transient radical anion reflects the high electrolysis efficiency of the gold-micromesh working electrode employed in this spectroelectrochemical study.

***g* Values**. The g values of π-conjugated organic radical ions can be smaller or larger than 2.0023 (g_e), according to whether the excited states that mix in with the ground state are from excitation of a singly occupied σ to empty π states or the inverse,[33] but either way the deviations are small: g values for radical anions of perylene (2.00267), diphenylacetylene (2.00264), and *trans*-stilbene (2.00270) are all slightly larger than g_e, while those of the nitrosobenzene radical cation (2.0007) and the benzoyl radical (2.0014) are slightly smaller.[33] The deviations in C,N,S radicals are much greater, with $g > g_e$. There is a general consensus that this is caused by excited states that mix spin−orbit coupling from the chalcogen into the g-tensor components, an effect that grows markedly with each subsequent chemical period.[28] The g values that we recorded for $\mathbf{1}^{\bullet-}$−$\mathbf{4}^{\bullet-}$ are similar to those of other C,N,S[34,35] and P,N,S[36] π-type ring systems. For compounds $\mathbf{1}^{\bullet-}$, they are invariant at 2.0087, while $\mathbf{2}^{\bullet-}$ resonates at lower field (g = 2.0094), and $\mathbf{3}^{\bullet-}$ (g = 2.0084) and $\mathbf{4}^{\bullet-}$ (g = 2.0065) resonate at higher field. While it is tempting to try to relate the significant variations in g to substituent effects (e.g., in $\mathbf{2}^{\bullet-}$) or with structure type ($\mathbf{3}^{\bullet-}$ and $\mathbf{4}^{\bullet-}$), not enough is known about the effects of either factor on the g tensors of such heterocycles to guide such interpretations. This is unfortunate, as this knowledge could assist with determining the solution structures of $\mathbf{1}^{\bullet-}$−$\mathbf{4}^{\bullet-}$ (see below).

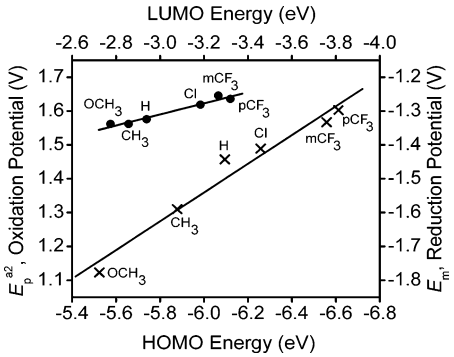

Figure 9. Plots of the calculated HOMO orbital energies of **1a**−**f** versus the CH_3CN voltammetric peak potentials derived for oxidation (×, bottom and left legends), and LUMO orbital energies of **1a**−**f** versus the midpoint potentials for reduction (•, top and right legends). The graph scale increments for the two plots are identical.

Effect of Substituents on the First-Reduction Process. For a closely related series such as **1a**−**f**, it is possible to look for a coherent influence of the substituents on the $E^{0/}$ value for their reduction (here assumed to correspond to the midpoint potentials E_m in Table 1). To a first approximation, the ease of adding an electron to **1** should depend on the energy of the acceptor molecular orbital, the LUMO of the neutral molecule (Figure 1b). Coherent dependences of this type have been observed previously for 1,2,3,5-dithiadiazolyl radicals bearing the same sets of para-aromatic substituents.[3,25] For the latter ring system, a good correlation was also established against the adiabatic ionization energies measured by UV-PES.[34] Other workers have demonstrated good correlations between dithiadiazolyl redox potentials and Hammett $\sigma_{m,p}$ constants.[25,37] We have therefore plotted the E_m potentials against the LUMO energies and the $\sigma_{m,p}$ constants. All the fits are reasonable (Supporting Information, Figures S1 and S2), but the best correlation is found with the orbital energies (Figure 9). Despite the sometimes less than ideal electrochemical response in CH_3CN and concomitant uncertainty in the thermodynamic significance of the E_m value, there is a good linear correlation of this parameter and the LUMO energy for the CH_3CN data reported in this paper (Table 6 and Figure 9) and a better correlation than with the potentials previously reported using CH_2Cl_2 as

(32) When a voltammetric process is chemically irreversible, it is not possible to ensure that the peak potential provides an exact guide to the value of the applied potential that should be used in a SEEPR experiment that is aimed at obtaining the radical anion.

(33) Goldberg, I. B.; Bard, A. J. *Chem. Phys. Lett.* **1970**, *7*, 139.
(34) Boeré, R. T.; Oakley, R. T.; Reed, R. W.; Westwood, N. P. C. *J. Am. Chem. Soc.* **1989**, *111*, 1180.
(35) (a) Boeré, R. T.; Roemmele, T. L. *Phosphorus, Sulfur Silicon Relat. Elem.* **2004**, *179*, 875. (b) Cordes, A. W.; Koenig, H.; Oakley, R. T. *J. Chem. Soc., Chem. Commun.* **1989**, 710. (c) Hayes, P. J.; Oakley, R. T.; Cordes, A. W.; Pennington, W. T. *J. Am. Chem. Soc.* **1985**, *107*, 1346.
(36) (a) Cordes, A. W.; Goddard, J. D.; Oakley, R. T.; Westwood, N. P. C. *J. Am. Chem. Soc.* **1989**, *111*, 6147. (b) Oakley, R. T. *J. Chem. Soc., Chem. Commun.* **1986**, 596.
(37) (a) Aherne, C. M.; Banister, A. J.; Gorrell, I. B.; Hansford, M. I.; Hauptman, Z. V.; Luke, A. W.; Rawson, J. M. *J. Chem. Soc., Dalton Trans.* **1993**, 967. (b) Swain, C. G.; Lupton, E. C. *J. Am. Chem. Soc.* **1968**, *90*, 4328. (c) McDaniel, D. H.; Brown, H. C. *J. Org. Chem.* **1958**, *23*, 420.

Table 5. Comparative Energies for Planar and Folded Conformations[a]

	ΔH(planar−folded) (kJ mol^{-1})	
compd	neutral	anion
1a	−29.8	−8.6
1b	−91.0[b]	−67.4[b]
1c	−35.8	−10.5
1d	−36.9	−11.1
1e	−40.7	−7.1
1f	−39.7	−17.2
2	−37.1	−5.9
3	34.3	44.2
4	128.2	95.2

[a] Values are obtained from the total energies with added zero-point energy corrections; a negative sign indicates a preference for a planar geometry. Energy minima are also available (Supporting Information, Table S2). [b] The reasons for the apparently anomalous values for **1b** and **1b**$^{-\bullet}$ have not been ascertained.

Table 6. Orbital Energies Determined from B3LYP/6-31G(d) Calculations for **1a**−**f**

substituent	LUMO energy (eV)	reversible reduction potential (E_m) (V)	HOMO energy (eV)	oxidation peak potential (E_p^a) (V)
4-OCH_3	−2.775	−1.338	−5.524	1.123
4-CH_3	−2.857	−1.338	−5.878	1.310
4-H	−2.939	−1.324	−6.095	1.457
4-Cl	−3.184	−1.281	−6.258	1.489
3-CF_3	−3.265	−1.254	−6.558	1.567
4-CF_3	−3.320	−1.264	−6.612	1.603

solvent.[5b] The small but definite change in E_m when the substituent is changed from electron-donating to electron-withdrawing is consistent with the nature of the LUMO (Figure 1b), which is nodal at carbon and highly localized on the $C_2N_4S_2$ ring. Therefore, only a mild inductive effect on the electronic structure from the remote aryl substituents may be expected, in line with similarly modest inductive effects observed on the SOMO redox orbital of dithiadiazolyls.[3,25]

The reduction of **2** (−1.46 V) occurs at a more negative potential than that of the aryl derivatives **1** (average value of ca. −1.3 V), reflecting the difference in inductive influence of *tert*-butyl and aryl substituents. However, a much larger negative shift in potential is observed in the folded dithiatetrazocines **3** and **4**, which undergo the first reduction at ca. −1.7 V. This may be due to substituent influence (dimethylamino is known to be a powerful donor) but might also reflect the intrinsic electronic properties of the folded geometry.

Effect of Substituents on the Oxidation Process. The irreversible nature of the oxidation processes of all the heterocycles studied here suggests that the initially formed oxidized species are chemically unstable under conditions of cyclic voltammetry in CH_3CN or CH_2Cl_2. It may be noted, however, that **3** and **4** are readily oxidized by halogens (Cl_2 or Br_2) in CH_3CN or CH_2Cl_2 or by the strong one-electron radical oxidant bis(trifluoromethyl)nitroxide in CCl_4 to give stable derivatives of the (formal) dications.[1,7a,b,8a] In strong contrast to this behavior, the planar **1c** resists these same oxidants entirely, even under forcing conditions (e.g., suspension in liquid Cl_2).[7] By analogy with the discussion presented for the first-reduction process and assuming that the kinetic terms are approximately constant, the relative values of the peak potentials for the oxidation process should have thermodynamic significance and hence reflect the relative energies of the HOMO (Figure 1a). Therefore, we plotted the peak potentials for these irreversible oxidation processes against the HOMO energies from the DFT calculations. An approximately linear correlation is indicated (Figure 9). We note that the fit to the CH_3CN data reported here is considerably better than that for the earlier data obtained in CH_2Cl_2, perhaps because the shifted peak potentials are more closely related to thermodynamically relevant ones. (Because the solvent with the higher dielectric constant may be better able to stabilize the putative cations or dications produced in these reactions.) The much larger range of measured peak potentials for oxidation and calculated HOMO energies, compared with the corresponding situation prevailing for the reduction, indicates that the oxidation is much more strongly influenced by the aryl group substituents. This effect is entirely consistent with the electronic structure of the HOMO (Figure 1a), which is calculated to be delocalized over the whole ring system, and not isolated to the central N_4S_2 region by nodal character. The difference between the influence on reduction and on oxidation is strikingly evident from the different slopes of the two lines in Figure 9.

We also note that the relative ease of the chemical oxidation of **3** and **4** compared with that of **1c** cannot be explained on the basis of peak potentials (assumed to be related to the reversible potentials), at least in CH_3CN, because the peak potential for the oxidation of **3** is very close to that of **1c**, while **4** has a lower peak potential than either of these two. The origin of the resistance of **1c** to chemical oxidation is therefore most probably located in kinetic rather than thermodynamic considerations, and hence, the description of the planar type **1** and **2** rings as 10π "aromatic" Hückel systems is substantiated by electrochemistry.[38]

Further Characterization of Redox Processes. CV studies on **3** in CH_3CN revealed a second fully irreversible reduction process. While there is no direct chemical evidence for the existence of such a dianion assumed to be initially formed in this process (in contrast to **4**), such a species formally exists in several metal adducts following the formal oxidative addition of the transannular S···S "bond" to zerovalent metals.[9a,39]

$\Delta E_{(ox-red)}$ values for **1a**−**f** in both CH_3CN and CH_2Cl_2 increase as the substituent is changed from electron-donating to electron-withdrawing. This variation largely reflects the strong substituent influence on the oxidation peak potentials, even though both the reduction and oxidation processes do shift in the same absolute direction. The large difference in $\Delta E_{(ox-red)}$ values is to be contrasted with the almost invariant $\Delta E_{(ox-red)}$ values observed for 1,2,3,5-dithiadiazolyls, the latter attributable to redox processes that involve

(38) Fowler, P. W.; Rees, C. W.; Soncini, A. *J. Am. Chem. Soc.* **2004**, *126*, 11202.
(39) (a) Chivers, T.; Hilts. R. W. *Inorg. Chem.* **1992**, *31*, 5272. (b) Chivers, T.; Dhathathreyan, K. S.; Ziegler, T. *J. Chem. Soc., Chem. Commun.* **1989**, 86.

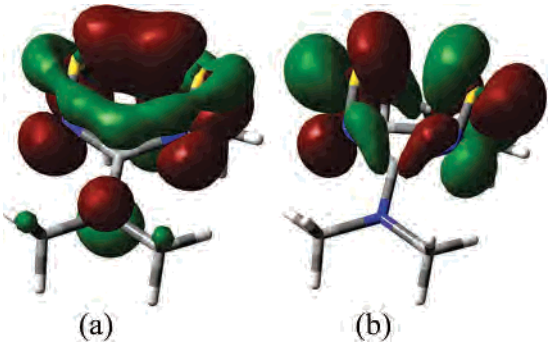

Figure 10. The Kohn−Sham orbital isosurfaces of the (a) HOMO and (b) LUMO of **3**.

the same redox SOMO rather than two different redox orbitals as in **1**.[3]

Structures of the Radical Anions. We have considered two options for the structures of the radical anions $\mathbf{1}^{\bullet-}-\mathbf{4}^{\bullet-}$: first, that they retain the structure—planar or folded—of the parent molecule, or second, that they change—from planar to folded or from folded to planar, although we acknowledge that intermediate geometries may also exist.[7d] We find that the planar forms of **1** and **2** are the most stable, and the same is true for their radical anions (Table 5). For example, in the case of **1c**, the energetic preference is 35.8 kJ mol^{-1} for the planar conformation. However, the folded structures for **1** and $\mathbf{1}^{\bullet-}$ and **2** and $\mathbf{2}^{\bullet-}$ are also local minima that converge in DFT without imaginary frequencies. The preference for planar is considerably *smaller* in the radical anions, for example, in $\mathbf{1c}^{\bullet-}$ by only 10.5 kJ mol^{-1}, although the scatter in their data is considerable (Table 5). For **3** and **4**, the folded shapes are by far more stable than the planar alternatives for both the neutral and radical anion, and the alternative planar geometries appear to be transition states with imaginary frequencies that provide for facile conversion into the folded ground states. Furthermore, the preference for the folded geometry actually increases from the neutral to the anion for these compounds (ΔH(planar−folded) = 44.2 and 95.2 kJ·mol^{-1}, respectively). A previous investigation into the activation energies for ring inversion and methyl group rotation of the bent derivative **3** by both NMR experiments and HF/6-31G(*) calculations has also led to a planar intermediate geometry at higher energy (∼60 kJ mol^{-1}), albeit at this level of theory, no imaginary frequencies were obtained.[7d] The noted increase in the transannular S···S separation in the folded geometries calculated for all the radical anions is consistent with an additional electron populating the LUMO, which is antibonding with respect to this interaction (Figure 10), thus canceling out half of the transannular "bond" in these folded systems; nevertheless, the preference for the folded geometry is in all cases *greater* in the anionic state. All other geometry changes in the radical anions are also consistent with semi-occupancy of their particular SOMOs and do not call for further discussion.

We have calculated the hfc for the spin-active nuclei (^{14}N, $^{14}N_{exo}$, ^{31}P, ^{13}C, and ^{33}S) computationally using DFT methods whose reliability has been thoroughly tested,[28−31] but the results (Table 3) are anything but conclusive with respect to structural assignments. In all cases, the differences between the calculated values for the two geometries are certainly smaller than the typical accuracy of these methods. Over the whole range of the nine radical anions that we have examined, the fit for both nitrogen and phosphorus hfc is slightly better for the folded versus the planar conformation, with percent deviations in the range of 1.5−6.8% for ^{14}N and 16.8% for ^{31}P (folded), versus 5.4−51.5% for ^{14}N and 27.4% for ^{31}P (planar). Less-favorable agreement is found between the calculated hfc for the exocyclic nitrogen atoms in the folded conformer of $\mathbf{3}^{\bullet-}$ at 88% versus 14.3% in the planar form; however, the absolute deviation of 0.037 mT is within the range of that seen for ^{14}N in the other ring systems. DFT frequency calculations also indicate that, whatever geometry is adopted, the radical anions have low deformation energies and each has several vibrational modes that interconvert the planar and folded conformations.

In the absence of a definite conformational assignment from the nitrogen and phosphorus coupling constants, we were very pleased to be able to obtain a high-quality EPR spectrum of $\mathbf{1c}^{\bullet-}$ generated in CH_3CN solution and for which the major lines do not obscure all the satellite lines from coupling to the low-abundance nuclei. In attempting to simulate these small satellites (see Figure 6), we found that it was necessary to use the combined intensity of all the remaining nuclei, that is, ^{15}N, ^{33}S, and ^{13}C, to be able to match the relative high intensities of these peaks. The best fit was obtained with hfc to all of these nuclei at ca. 0.55 mT, values which in the case of the ^{13}C coupling are more consistent with a result derived from a folded conformation. However, the spectral assignment still remains uncertain given the very small size of these natural-abundance lines in the presence of the high-intensity ^{14}N lines. We estimate that a definitive assignment of the ^{13}C hfc would require at least 10−20% enrichment in ^{13}C content.

Possible Mechanisms for the Follow-Up Chemical Reaction. The radical anions $\mathbf{1}^{\bullet-}-\mathbf{4}^{\bullet-}$ are transient species (see Table 4); any hope of isolating any one of them for the purpose of obtaining their structures by conventional means is slim indeed. Save for $\mathbf{4}^{\bullet-}$, the rate constants for the decay of the anion radical are roughly comparable (with half-lives ranging from 10 to 35 s). Electrochemical measurements of the rate constants were done only for anion radicals $\mathbf{1c}^{\bullet-}$ and $\mathbf{3}^{\bullet-}$, and the result is in good agreement with the values determined by EPR (see Table 4). The electrochemical data, obtained at two different concentrations (see Table 2), strongly support the contention that the decay process is first order. The linearity of the semilog plots of the intensity of the EPR signal vs time (see Figure 7) also supports the contention that the decay process is first order.

When thinking about the nature of the follow-up reaction, the following pieces of evidence need to be taken account of: (1) A unimolecular decomposition is the most likely chemical path in view of the first-order kinetics; (2) decomposition of $\mathbf{1}^{\bullet-}-\mathbf{4}^{\bullet-}$ leads to the loss of all EPR signal intensity; and (3) the rates measured for the series of compounds, despite the possible presence of two conformational states, are remarkably similar. First of all, radical−radical coupling, one commonly observed EPR decay mechanism, seems to be ruled out, since that demands second-order kinetics. This seems reasonable since dimerization to form a dianion is unlikely. We note, however, that 6-to-12 ring enlargement reactions have been observed for

Scheme 2

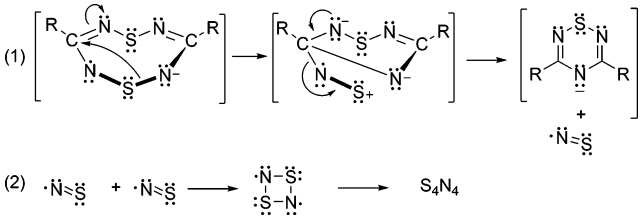

diphosphathiatriazines in other cases.[40] When searching for possible analogies to the reactions of our systems, the only well-characterized example that we are aware of is the decomposition of $[S_4N_4]^{-\bullet}$. Williford et al. have demonstrated from voltammetry and EPR spectroscopy that the decay of this unstable anion is also first order and involves the loss of all EPR signal intensity.[41] At the same time, Chivers and Hojo demonstrated by polarography and exhaustive electrolysis that the end product of $[S_4N_4]^{\bullet-}$ reduction is the quantitative formation of $[S_3N_3]^-$.[42]

Rearrangements have been shown to occur between sulfur diimides and their radical anions[43] and the 1,3,2,4-dithiadiazolyls,[44] both involving 1,2 N,S shifts controlled by the topologies of the frontier orbitals. The 1,3 nitrogen shift mechanism has been shown to operate in neutral sulfur nitrogen ring and cage compounds, in particular when they are subjected to nucleophilic attack. This process facilitates nitrogen scrambling at room temperature and below in solution for $PhCN_5S_3$ cage molecules[45] and provides a facile, low-temperature, pathway for the endo/exo isomerization of certain trithiatetrazocines, by the interconversion of six- and eight-membered rings.[46] A plausible mechanism for the decay of $[RCN_2S_2N_2CR]^{\bullet-}$ employing such a 1,3 nitrogen shift mechanism is drawn in Scheme 2.

This mechanism proceeds via a four-coordinate carbon center, which is known to occur in the transition states for the nitrogen-scrambling reactions of $PhCN_5S_3$.[45] The end product after the elimination of $SN^{\bullet}$ (predicted to be EPR silent in condensed phases)[30] is the anion of a 1,2,4,6-thiatriazinyl. In the specific case of R = Ph, such an anion has actually been isolated, but only in its protonated (imine) form when generated in liquid ammonia in the presence of excess H^+.[47] It is certainly possible that under the conditions of our voltammetric and SEEPR experiments this thiatriazinyl anion is unstable and will decompose further, with a nitrile and more $SN^{\bullet}$ as the final products of electrolysis. However, in the absence of experimental evidence for the decay products, further speculation is not warranted at this time.

Conclusions

The application of the technique of in situ EPR spectroelectrochemistry has led to the conclusive identification of radical anions $\mathbf{1}^{\bullet-}-\mathbf{4}^{\bullet-}$, which have not been detected previously. Single-scan EPR spectra with high signal-to-noise ratios have been recorded, despite half-lives as short as 1 s. Simulations of cyclic voltammetric responses for **1c** and **3** in CH_2Cl_2 verify the electrochemical reversibility of the reduction process, as well as the irreversible chemical decay of the radical anion via a first-order reaction pathway, with rate constants in satisfactory agreement with those obtained by SEEPR experiments. Postulates for the decay of the radical anion are included, but the ultimate products are unknown. Trends in both the redox potentials and hfc constants for **1a**−**f** reflect the electronic influence of the remote aryl substituents. With respect to the structure of the radical anions, DFT calculations are inconclusive for $\mathbf{1}^{\bullet-}$ and $\mathbf{2}^{\bullet-}$ but suggest that $\mathbf{3}^{\bullet-}$ and $\mathbf{4}^{\bullet-}$ retain the folded geometry of the neutral structures. Analysis of EPR spectra obtained by enrichment of the dithiatetrazocine ring carbon atoms with ^{13}C (from the commercially available $Ph^{13}CN$) may resolve the structural dichotomy of $\mathbf{1c}^{\bullet-}$. It is anticipated that many new main-group free radicals may be identified using the SEEPR methodology described in this paper. Vigorous efforts are underway in our laboratories to exploit the combined approach of voltammetry, SEEPR, and DFT calculations to characterize main-group element free radicals.

Acknowledgment. We wish to extend special thanks to Dr. Richard Webster (Nanyang University of Technology, Singapore), who provided advice on the working electrode that was used in the SEEPR experiments, Drs. Heikki Tuononen (University of Jyvaskalä, Finland) and Stacey Wetmore (University of Lethbridge) for help with the DFT calculations, and C. Bumbac (University of Calgary) for the preparation of compound **4**. Financial support from the Natural Sciences and Engineering Research Council-Canada (T.L.R., R.T.B., and T.C.) and the Alberta Ingenuity Fund (T.L.R.) is gratefully acknowledged. This project was initiated through a Linkage International award from the Australian Research Council (R.T.B. and A.M.B) and supported through a visiting fellowship to R.T.B. from the Research School of Chemistry of the Australian National University. We thank the anonymous reviewers for helpful suggestions.

Supporting Information Available: Comparative bond lengths and angles of the neutral compounds in the solid state versus DFT optimized geometries (Table S1); DFT computed energies for the two conformations considered for the radical anions (Table S2); comparison of experimental and calculated interatomic distances and angles for the neutral and radical anions (Tables S3 and S4); correlation plots of the Hammett coefficients versus the oxidation and reduction potentials of **1a**−**f** (Figures S1 and S2). This material is available free of charge via the Internet at http://pubs.acs.org.

IC070243T

(40) (a) Chivers, T.; Rao, M. N. S. *Inorg. Chem.* **1984**, *23*, 3605. (b) Chivers, T.; Rao, M. N. S.; Richardson, J. F. *J. Chem. Soc., Chem. Commun.* **1983**, 186. (c) Oakley, R. T. *J. Chem. Soc., Chem. Commun.* **1986**, 596.

(41) Williford, J. D.; Van Reet, R. E.; Eastman, M. P.; Prater, K. B. *J. Electrochem. Soc.* **1973**, *120*, 1498.

(42) Chivers, T.; Hojo, M. *Inorg. Chem.* **1984**, *23*, 1526.

(43) Bestari, K.; Oakley, R. T.; Cordes, A. W. *Can. J. Chem.* **1991**, *69*, 94.

(44) (a) Burford, N.; Passmore, J.; Schriver, M. J. *J. Chem. Soc., Chem. Commun.* **1986**, 140. (b) Passmore, J.; Sun, X. *Inorg. Chem.* **1996**, *35*, 1313.

(45) (a) Boeré, R. T.; Oakley, R. T.; Shevalier, M. *J. Chem. Soc., Chem. Commun.* **1987**, 110. (b) Bestari, K. T.; Boeré, R. T.; Oakley, R. T. *J. Am. Chem. Soc.* **1989**, *111*, 1579.

(46) (a) Boeré, R. T.; Cordes, A. W.; Craig, S. L.; Graham, J. B.; Oakley, R. T.; Privett, J. A. J. *J. Chem. Soc., Chem. Commun.* **1986**, 807. (b) Boeré, R. T.; Cordes, A. W.; Oakley, R. T. *J. Am. Chem. Soc.* **1987**, *109*, 7781.

(47) Boeré, R. T.; Cordes, A. W.; Hayes, P. H.; Oakley, R. T.; Reed, R. W.; Pennington, W. T. *Inorg. Chem.* **1986**, *25*, 2445−2450.